2019•2020

Faculteit Industriële ingenieurswetenschappen

master in de industriële wetenschappen: chemie

Masterthesis

Development of a copper doped birnessite manganese dioxide cathode for aqueous zinc-ion batteries

PROMOTOR :

Prof. dr. ir. Leen BRAEKEN

PROMOTOR :

Prof. dr. Thuy HOANG THI BICH

COPROMOTOR :

ir. Thu HANG LE THI

Leandro Schepers

Scriptie ingediend tot het behalen van de graad van master in de industriële wetenschappen: chemie

Gezamenlijke opleiding UHasselt en KU Leuven

2019•2020

Faculteit Industriële ingenieurswetenschappen

master in de industriële wetenschappen: chemie

Masterthesis

Development of a copper doped birnessite manganese dioxide cathode for aqueous zinc-ion batteries

PROMOTOR :

Prof. dr. ir. Leen BRAEKEN

PROMOTOR :

Prof. dr. Thuy HOANG THI BICH

COPROMOTOR :

ir. Thu HANG LE THI

Leandro Schepers

Scriptie ingediend tot het behalen van de graad van master in de industriële wetenschappen: chemie

UHASSELT KU LEUVEN

Deze masterproef werd geschreven tijdens de COVID-19 crisis in 2020. Deze wereldwijde gezondheidscrisis heeft mogelijk een impact gehad op de opdracht, de onderzoekshandelingen en de onderzoeksresultaten.

1 ACKNOWLEDGMENTS

I have written this master thesis during the course of my final year at the university of Hasselt and the catholic university of Leuven in fulfilment of the requirements to obtain the degree of Master of Science in Chemical Engineering Technology.

The idea for this master thesis goes back to the classes of Professor Braeken at the University of Hasselt, Professor Braeken covering the field of electrochemistry. Her clear analysis of the course inspired me to read up on the subject. Professor Braeken's empathic and thoughtful guidance, assistance and dedication enabled me to overcome a number of important hurdles on my way to completing this thesis. Her unwavering enthusiasm encouraged me to continue my research under adverse external circumstances, most notably the Covid-19 pandemic. Therefore, Professor Braeken, thank you!

I would also like to thank my External Promoter, Professor Thuy Hoang of the Hanoi University of Science and Technology, who guided me intensively during my stay in Vietnam and helped me integrate into the group.

For sure, I would also like to express my gratitude towards Kenneth Put for the friend he has been throughout the years. I will always remember the wonderful time we have had together in Vietnam.

Finally, I wish to thank my loving parents and my sister, for their understanding, support and encouragement during my entire education. To them this thesis is dedicated.

Leandro Schepers

Heusden-Zolder, 2020

.

2 LIST OF CONTENTS

3 LIST OF TABLES

4 LIST OF FIGURES

5 NOMENCLATURE

Symbol	Meaning
A	surface area of the electrode
a_{ox}	activity of the oxidant
a_{red}	activity of the reductant
c	specific capacity
c_j^0	initial concentration of the reducible analyte j in mol/cm³
C^e	Concentration of ions at the closest approachable distance of an ion
C^b	concentration of an ion in the bulk
D_j	diffusion coefficient for species j in cm²/s
E	voltage
E_0	standard potential
F	Faraday's constant
i	current in Ampère
I_p	peak current in a cyclic voltammetry test
M	Molar mass
n	Amount of electrons
R	gasconstant in J/(K*mol)
T	temperature in Kelvin
t	time in seconds
v	scan-rate in V/s
ϕ^e	potential difference over the double layer capacity

6 ENGLISH ABSTRACT

This thesis describes a pathway towards developing a suitable cathode material for zinc-ion batteries. During recent years, the demand for new rechargeable battery types as a replacement for lithium-ion batteries has increased continually as a result of the shortage of lithium in the Earth's crust and the increase of renewable energy sources that need large energy storage systems. One of the most promising alternatives are zinc-ion batteries. However, finding a suitable cathode material has proven to be a considerable challenge.

In the framework of my thesis, I will evaluate the suitability of the cathode material by using cyclic voltammetry to determine the cyclability of the cathode, XRD and SEM to investigate the cathode material's structure and electrochemical impedance spectroscopy to measure characteristic resistances of the cathode.

I will identify δ-manganese dioxide as the most promising cathode material. Doping this cathode with copper increases its conductivity, which should result in a battery with a higher energy storage capacity than before. The cathode material is synthesised through a redox precipitation reaction. The cathode material may suffer from poor mechanical stability, so further research that uses the idea of copper doping in combination with a reinforced structure, like polyaniline-intercalated manganese dioxide, could result in a full-fledged cathode material.

7 DUTCH ABSTRACT

Dit proefschrift beschrijft een methode voor het ontwikkelen van een geschikt kathodemateriaal voor zink-ion batterijen. De laatste jaren is de vraag naar nieuwe soorten oplaadbare batterijen als vervanging voor lithium-ion batterijen gestaag toegenomen als gevolg van het tekort aan lithium in de aardkorst en de toename van hernieuwbare energiebronnen die grote energieopslagsystemen vereisen. Een van de meest veelbelovende alternatieven zijn zink-ion batterijen. Het vinden van een geschikt kathodemateriaal is echter een aanzienlijke uitdaging gebleken.

In het kader van mijn proefschrift zal ik de geschiktheid van het kathodemateriaal evalueren aan de hand van cyclische voltammetrie om de herlaadbaarheid van de kathode te bepalen, XRD en SEM om de kristalstructuur van het kathodemateriaal te verifiëren en elektrochemische impedantie spectroscopie om karakteristieke weerstanden van de kathode te meten.

Ik kom tot de conclusie dat δ-mangaandioxide het meest veelbelovende kathodemateriaal is. Het doteren van deze kathode met koper verhoogt de geleidbaarheid van het materiaal, hetgeen zou moeten resulteren in een batterij met een hogere energieopslagcapaciteit dan voorheen. Het kathodemateriaal wordt gesynthetiseerd via een redox-precipitatiereactie. Het valt te verwachten dat de δ-mangaandioxide-kathode aan een slechte mechanische stabiliteit lijdt. Verder onderzoek dat het idee van koperdopering gebruikt in combinatie met een versterkte structuur, zoals polyaniline-geïntercaleerd mangaandioxide, zou kunnen resulteren ineen volwaardige kathode.

8 PROJECT GOAL

8.1 CONTEXT

Batteries have always been used as portable energy storage devices. As of this era, another application for batteries is speculated about. Since the whole world is transforming its energy grid from non-renewable to renewable, existing renewable energy sources rely mostly on solar and wind energy [1]. It is well known that these are unreliable energy sources as they alternate with sun or wind activity. One of the most convenient solutions is the use of mega-batteries, which can transform electric energy into chemical energy when there is an abundance of solar and wind energy. They can deliver this energy back to the grid whenever there is an energy deficit.

For these batteries to be worth producing, it is vital that the raw materials used are non-toxic, cheap [2] and reliable. A battery-type that is very promising is the zinc-ion battery. Zinc is relatively cheap and safe [3]. This makes it suited as anodic material.

However, as zinc is only the anode, the development of good cathodes is also necessary. Cathodes have a large impact on the quality of batteries. In case of zinc-ion batteries it has proven to be a challenge to come up with a cathode material that undergoes reversible electrochemical reactions. The most applied cathode material for rechargeable zinc-ion batteries is manganese-dioxide.

The aim of this research is to develop a structure of manganese dioxide that has a long life cycle and high capacity (mAh/g).

8.2 PROBLEM STATEMENT

Zinc-ion batteries are currently not widely used for several reasons. The first one is the formation of dendrites at the surface of the zinc-anode. Dendrites form slowly during charging and result in many disadvantages as described by Lu et al “dendrites will lead to the loss in the efficiency and capacity of batteries. The continual growing dendrites will finally pierce the separator and cause the short circuit of batteries.” [4]. The loss of capacity is a result of dendrites breaking off from the anode. These broken-off dendrites are not connected with the circuit anymore and therefore not electrically active. The batteries also malfunction when a dendrite does not break lose but pierces the separator, resulting in a short circuit. Many inhibitory resistors already have been posed in order to solve this problem [5].

A second weak element of zinc-ion batteries is the low conductivity of the cathodes. MnO_2, which has been investigated as cathode material because of its high capacity, also suffers

strongly from this issue. MnO_2 also creates partly irreversible structures when discharged. This leads to capacity loss and a poor life cycle because those structures are not electroactive [6] [7].

δ-manganese dioxide has emerged as promising cathode material due to its high capacity. However, it suffers from the same problems as described above and also reveals poor (thermal) stability. The reason according to Liu et al for this poor stability is still unknown [8].

8.3 OBJECTIVES

This thesis provides a method to improve the conductivity of δ-manganese dioxide. Accordingly, a δ-MnO_2 cathode material with high electrochemical performances can be obtained. To my best knowledge, it is the first time that doping δ-MnO_2 with copper has been investigated. This aims to increase conductivity of δ-MnO_2. Other researchers already reported positive results on other polymorphs of MnO_2 that are doped with copper, such as γ-MnO_2 [9]. Possibly, the stability will be improved by experimenting with ion exchange [8].

8.4 DESCRIPTION METHOD

In the first place, the synthesis method proposed by Schubert et al [10] will be followed. At the end of this process birnessite (δ-manganese dioxide) is formed. Birnessite is made out of stacked layers of MnO_2. The space between those layers (interlayers) is filled with solvated ions.

The interlayers, after the preparation of the birnessite, are filled with solved sodium ions. According to Feng et al the intercalation of sodium ions has a positive impact on the capacity of sodium batteries [11]. When applying this idea to zinc batteries, an ion exchange is conducted to replace the sodium ions with zinc ions. Ching et al reported that by aging the birnessite for 24h in a bath containing 1M of a cation the interlayer ion exchange will succeed [12].

To test the synthesized manganese dioxide, cyclic voltammetry tests will be conducted on the samples. Cyclic voltammetry gives an inside in the stability of the manganese dioxide. A second test that will be carried out is Electrochemical Impedance Spectroscopy test. The test allows the resistance (which is the inverse of the conductivity) to be studied very specifically. “More specifically allowing to separate the influences of different components that means the contribution of the electron transfer resistance, double layer capacity, etc” [13]. Other important tests are XRD and SEM. Comparison between an XRD result of the prepared samples and XRD patterns derived from the reported literature will confirm whether the lattice structure of the synthesized sample is birnessite [14]. If these XRD patterns indeed match, a SEM-analysis will be carried out. This will give an image which can provide even more precise information about the morphology and structure of the obtained birnessite.

9 LITERATURE STUDY

9.1 BATTERY CONCEPT

The core principle of a battery is the conversion of chemical energy in electrical energy. This relies on a redox reaction in which an oxidation reaction and a reduction occur. Both reactions happen spontaneously and cause an electron transfer. This electron transfer action is the electrical current, thus energy that is produced.

The redox reaction is often performed in a galvanic cell. In this cell, there are two metallic plates from different metals. In order to form a closed circuit, a part of the plates is connected by a wire and another part is connected to an electrolyte. A common example is the galvanic cell of copper and zinc. As can be seen in Figure 1, both electrodes are placed in a electrolyte solution. The two sides of the electrolyte are separated by a membrane. The objective of the membrane is to prevent the cations, which can deposit on the electrodes, to migrate to the other side of the cell.

When the circuit is closed (see Figure 1), electrons flow from the anode side to the cathode side. Herein, zinc is the oxidizing agent and copper is the reducing agent. When the electrons from the anode reach the cathode, copper ions from the electrolyte are reduced and deposit on the cathode. In order to keep the whole system electrically neutral, ions in the solution migrate.

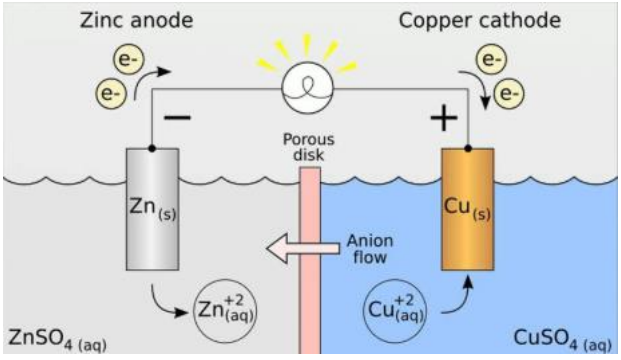

Figure 1. Electrochemical cell [15]

Batteries are generally one or multiple galvanic cells. They include an anode, a cathode and an electrolyte. The wire is normally expanded with a load that needs the power supplied by the battery. Nowadays, popular batteries use lithium, lead or zinc as anode, and carbon or transition-metal oxides as cathode. The most common battery-types are: Lead-acid, Ni-Cd, Ni-metal hydride (Ni-MH) and zinc-carbon batteries (a more comprehensive description of the types will be given at Types of batteries).

9.2 HISTORY OF THE BATTERY

9.2.1 Voltaic pile

In the year 1800 Alessandro Volta described the first apparatus capable of producing a constant electrical power. It consisted out of two discs, one made from zinc or tin and the other made from silver or copper. Both discs were separated by water-soaked paper that served as an electrolyte medium. This formed an electrical cell. The pile was constructed by stacking several of these cells on each other. When the pile was discharged, the Tin/Zinc discs were corroded. At that time, this led to the assumption that the Tin/Zinc plates were the only electrochemical active plates.

The oxidation reaction that occurred in the pile was described as follows:

$$Zn \rightarrow Zn^{2+} + 2e^-$$

and the reduction reaction was described as:

$$2\ H_3O^+ + 2\ e^- \rightarrow H_2 + 2\ H_2O$$

The cathode material itself was not the electroactive chemical because of the lack of copper/silver cations in the water of the soaked-paper.

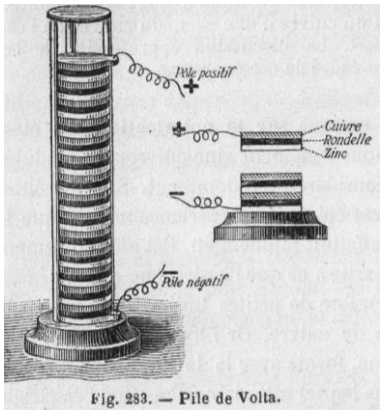

Fig. 283. — Pile de Volta.

Figure 2. Voltaic pile [16]

Even though the Voltaic pile was a great success, it also had its limitations. The first one was its short lifetime. Because of the fact that electrochemical reactions in Voltaic cells were surface reactions and the amount of reactive surface decreased due to corrosion, the output power of those cells rapidly declined. The second problem was that the weight of the pile drained the soaked paper what caused electrolyte leakage [17]. A final problem was the big influence of activation polarization (See Activation polarization) caused by the hydrogen gas.

9.2.2 Trough battery

As mentioned, the corrosion of the anode is a limiting factor for the operation of the voltaic pile. Cruickshank offered a solution for this problem with his new battery design, nowadays called the trough battery. The body of the battery is made out of a wooden trough with grooves in it. The grooves are filled with soldered plates of copper and zinc. Between the soldered plates an ammonium nitrate solution is present to replace the soaked-paper from

the Voltaic pile. This build up allows the corroded anode surface to be cleansed by acid as shown in the reaction below. Thereby, it offered a solution for the corrosion problem of the Voltaic pile. The design of the battery also allowed it to lay down. This prevented leakage of electrolyte.

$$Zn(OH)_2 + H_2SO_4 \rightarrow ZnSO_4 + 2H_2O$$

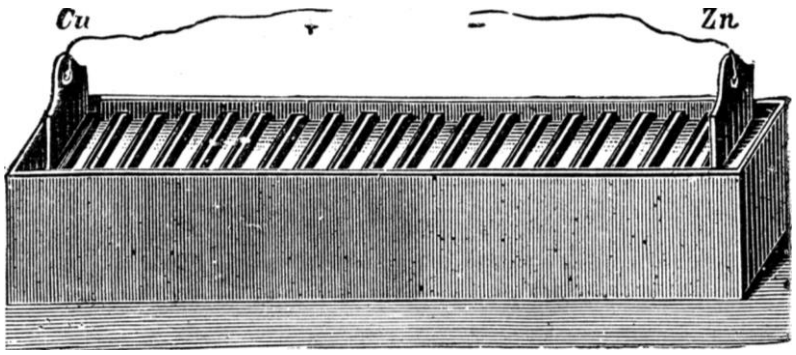

Figure 3. Trough battery [17]

9.2.3 Daniell cell

The Daniell cell is an invention of John Frederic Daniell in 1836. The cell has a simple construction. In the centre of the cell, there is a zinc rod surrounded by a solution of sulfuric acid. A membrane shields the solution from the rest of the cell, existing out of a copper cylinder and a copper(II)sulphate solution. The whole cell is kept together by being placed in a beaker (J in Figure 4).

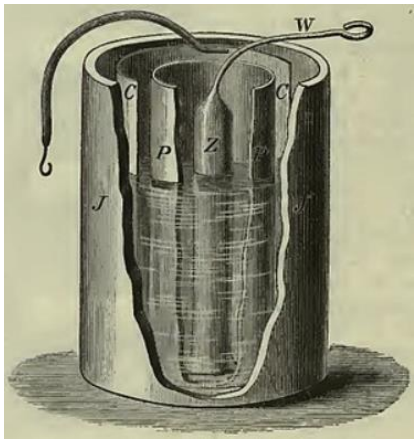

Figure 4. Daniell cell [18]

Contrary to the Voltaic pile, the cathode reaction was not the formation of hydrogen gas but rather the reduction of Cu^{2+} to Cu(s). The overall discharging reaction can be expressed as follows:

$$Zn + Cu^{2+} \rightarrow Zn^{2+} + Cu$$

This solved the problem of the formation of hydrogen gas what led to polarization. The design also made the battery much easier to transport.

In 1839 William Grove presented an improvement of the Daniell cell in which he replaced the copper cathode with a platinum one and changed the copper sulphate solution for nitric acid [19]. The cathode's active material is not platinum but the nitric acid, making the cathodic reaction:

$$2\ H^+ + 2\ HNO_3 + 2\ e^- \rightarrow 2\ H_2O + 2\ NO_2$$

Those changes resulted in the battery being capable of delivering a significant higher current and voltage than before. Originally, an output voltage of 1.1V was achieved as a result of the redox potential voltage difference of copper and zinc, respectively +0.34V and -0.76V (appendix 1). The voltage increased to 1.9V, because the redox potential of the nitrate/ nitrogen is, based on Dutton et al [20], around +1.3V. The expensive platinum cathode was chosen for its highly conductive and inert characteristics. Later improvements of the Daniell/Grove cell consisted of the replacement of expensive platinum cathode material by cheaper materials like carbon.

9.2.4 Lechlanché cell

The Grove cell had the disadvantage of having a liquid electrolyte. This made the cell heavy and therefore unusable as a mobile battery. The solution also contained strong acids which caused high safety risks. Georges Lechlanché proposed a solution for this. He still used a zinc rod as anode but replaced the cathode with a ceramic pot filled with a mixture of carbon and manganese(IV)oxide. He replaced the sulfuric acid solution with a solution of ammonium chloride, which resulted in a much safer battery and also increased the stability of the cell. An increased stability means, in this case, that the voltage the cell provided stayed more constant over time.

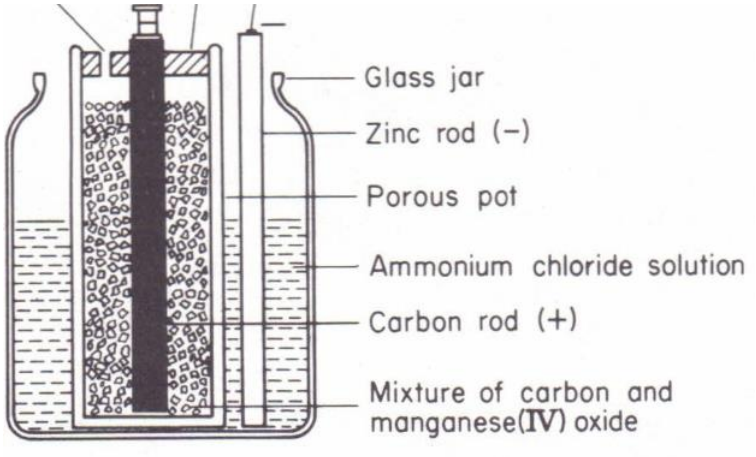

Figure 5. Lechlanché cell

The overall cell reaction occurring in the battery was expressed as:

$$Zn + 2\ NH_4^+ + 2\ MnO_2 \rightarrow Zn^{2+} + 2\ Mn(OOH) + 2\ NH_3$$

Later in the eighties of the 19th century, many scientists and engineers designed batteries in which the electrolyte was immobilized, what led to the decrease of battery weight. Only much later, in 1949, Paul Marsal registered and was granted a patent for what can be seen as the first version of the modern zinc alkaline battery, where the case of the battery is the anode itself (zinc) [21]. Thereafter, further improvements were made over the years by a variety of different people and companies. This led to the development of lots of new batteries including non-rechargeable and rechargeable batteries and their relevant battery materials, for example, the nickel-metal hydride batteries.

9.3 CLASSIFICATION OF BATTERIES

9.3.1 Prerequisite of a reversible electrochemical reaction

To illustrate the prerequisite for an electrochemical reaction to be reversible, the reduction reaction will be examined. When the lowest unoccupied molecular orbital (LUMO) of a molecule has a lower energy level than the highest occupied molecular orbital (HOMO) of another molecule it becomes thermodynamically favourable for an electron exchange to happen. In a galvanic cell, this is what happens, even though there is no direct contact between the two electroactive components.

9.3.2 Primary batteries

Primary batteries are not able to reverse the reduction reaction that has happened. If the batteries get connected to an external power source, which imposes a potential on its anode and cathode, the electrons present in the anode are still at a lower energy level than the LUMO of the oxidized electroactive component. This means that no electron transfer will occur and thus that the reaction is not reversible. Batteries where this is the case, can only discharge once and are called primary batteries.

9.3.3 Secondary batteries

Secondary batteries (also referred to as rechargeable batteries) need to be able to reverse the reduction and oxidation reaction. If the batteries get connected to an external power source, which imposes a potential on its anode and cathode. The electrons present in the anode will be at a higher energy level than the LUMO of the oxidized electroactive component, resulting in an electron transfer [22]. Batteries that are able to also reverse the oxidized state of their reduced component are called secondary batteries.

9.4 ELECTROCHEMICAL REACTIONS

9.4.1 Nernst Equation

As every chemical reaction, electrochemical ones have an equilibrium. This means that at a certain temperature and voltage the amount of reduced and oxidized ions are in a dynamical balance. The equation that describes this balance is the Nernst equation (eq 1)

$$E = E_0 + \frac{R*T}{n*F} * \ln\left(\frac{a_{ox}}{a_{red}}\right) \quad (1)$$

E is the applied voltage, E_0 the standard potential and a_{ox} and a_{red} the activities of the respectively reduced and oxidized agents. In experiments, the activities usually are replaced by the concentrations, and the standard potential with the formal potential. The formal potential is the standard potential with a correction applied, based on the activity coefficients of the oxidant and the reductant. By using this equation, the shape of the cyclic voltammetry (see Cyclic voltammetry) results can be partly explained.

9.4.2 Intercalation and insertion

An intercalation/insertion mechanism is a reversible electrochemical reaction used in rechargeable lithium-ion batteries. During intercalation and insertion a matrix, most commonly made out of a metal oxide kept together via Van der Waals forces, is expanded by ions that intrude in between the metal oxide layers. If the matrix consists of planes of metal oxides, sometimes referred to as a 2D structure, the process is called intercalation. When the structure consists of fibers (1D) or tunnels (3D) the process is called insertion.

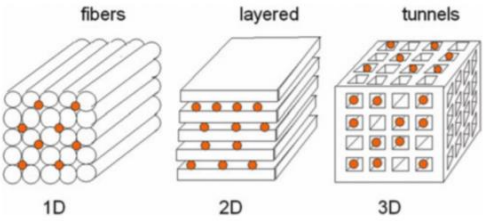

Figure 6: Dimensional structures for insertion/intercalation [21]

When these ions, mostly cations, intrude in the matrix, they cause an expansion of the interlayer distance. The energy for this widening is provided by a charge transfer reaction to the electroactive cations. The rate of the reaction is in normal circumstances determined by the transport properties from the bulk [23].

9.5 TYPES OF BATTERIES

9.5.1 Lead-acid battery

The lead-acid battery (LAB) is seen as the first good functioning secondary battery. It was invented in 1860 by Gaston Planté but only became a success 20 years later with the invention of Gramme machine [24]. LAB has the advantage of having a great cyclability performance and low cost. However, the battery is nowadays only used as car battery, because it has a low specific capacity, which means it needs to be quite heavy when applied. Another downside to the LAB is its long charge time (between 8 and 16 hours).

The anode of a LAB is made out of lead and the cathode out of lead dioxide. The electrolyte is a sulphuric acid solution. When the battery is discharging, the lead oxidizes and forms $PbSO_4$, simultaneously lead in lead dioxide reduces and forms lead sulphate [25]. The anodic and cathodic reactions are respectively:

$$Pb + H_2SO_4 \rightarrow PbSO_4 + 2\,H^+ + 2\,e^-$$

$$PbO_2 + H_2SO_4 + 2\ H^+ + 2\ e^- \rightarrow PbSO_4 + 2\ H_2O$$

9.5.2 Lithium-ion battery

Currently, the Lithium-ion battery is the most used battery for portable devices applications. More specific the lithium/manganese dioxide battery, which has the following corresponding intercalation reactions:

Cathode

$$MnO_2 + x\ Li^+ + x\ e^- \rightarrow Li_xMnO_2$$

Anode

$$Li \rightarrow Li^+ + e$$

Frost & Sullivan reported in 2018 that the lithium-ion battery market will grow towards 43.2 billion dollar in 2023 [26]. This makes it by far the largest battery market at the moment. Lithium-ion batteries are popular for their high energy density and reloadability. A comparison with other batteries as can be seen in Table 1.

9.5.3 Zinc alkaline battery

Zinc alkaline batteries (ZAB) are widely used as primary batteries, which means they can only discharge once. ZAB are single use batteries because they are cheap and safe, as they use an aqueous electrolyte and only zinc and a carbon/ MnO_2 / NH_4Cl mixture, with a carbon rod placed central, as respectively anode and cathode.

The general reactions of the cell are as follows:

Cathode

$$MnO_2 + H_2O + e^- \rightarrow Mn(OOH) + OH^-$$

Anode

$$Zn + 4\ OH^- \rightarrow Zn(OH)_4^{2-} + 2e^-$$

These batteries are used in a variety of applications. Generally they are used for apparatus that do not need a lot of energy and thus can function for a long time on one pair of batteries. By example a wireless controller for a television.

9.5.4 Nickel-cadmium battery

A nickel-cadmium battery (NCB) is constructed of an anode made from cadmium and a cathode made from nickel oxide hydroxide. This battery was frequently used in cheap toys and other apparatus that needed cheap rechargeable batteries. Since 2008, the European Union has forbidden the use of these batteries (apart from some exceptions) and has ordered its member states to implement Ni-MH batteries as substitution. [27] The reason for the ban is the toxicity of cadmium.

The cell half-reactions occurring in the NCB can be expressed as follows:

Cathode

$$Ni(OOH) + H_2O + e^- \rightarrow Ni(OH)_2 + OH^-$$

Anode

$$Cd + 2\ OH^- \rightarrow Cd(OH)_2 + 2\ e^-$$

9.5.5 Nickel-metal hydride battery

As mentioned above, nickel-metal hydride battery (NMHB) are used as replacement for the NCB. This means most of the applications are similar. The battery is also constructed of a nickel oxide cathode, but contrary to the NCB, the anode is made of a metal hydride. The metal itself is an alloy made from one-sixth lanthanum and five-sixth nickel. The reactions on the electrode surfaces are:

Cathode

$$Ni(OOH) + H_2O + e^- \rightarrow Ni(OH)_2 + OH^-$$

Anode

$$MH + OH^- \rightarrow M + H_2O + e^-$$

Table 1. Comparative scheme of different battery types

	Lead-acid battery	Li-ion battery	Zn alkaline battery	Ni-Cd battery	Ni-MH battery
cell-voltage (V)	2.1	3.6	1.5	1.2	1.2
specific energy (Wh/kg)	35-40	150-180	80	40-60	60-120
rechargeable	yes	yes	no	yes	yes
cost $/kWh	150-200	600-800	140	±230	400

9.6 BATTERY CHARACTERISTICS

9.6.1 Battery potential

As said before, batteries are in fact electrochemical cells, where oxidation and reduction reactions happen spontaneously. Both reactions have a value correlating to it, namely the standard half-cell potential. For a table of some half-cell potentials, see appendix 1. When two chemicals with each a different half-cell potential serve as electro-active material, the difference between the two half-cell potentials is the standard potential of the reaction. Combining these with the concentration of the electroactive species or the degree of occupancy for intercalation reactions, (y in Figure 7) the battery voltage in ideal circumstances can be determined via the Nernst equation, or for intercalation reaction via the formula in Figure 7. In order to take the interactions of species during insertion or intercalation into account an extra term, *Ky,* is added. Factor K is positive for attractive interaction and negative for repulsive interactions. The term n in Figure 7 is a constant that always takes the value 1 or 2, dependent on the cathode material. Finally, it needs to be pointed out that this equation is only valid for single electron intercalation reactions.

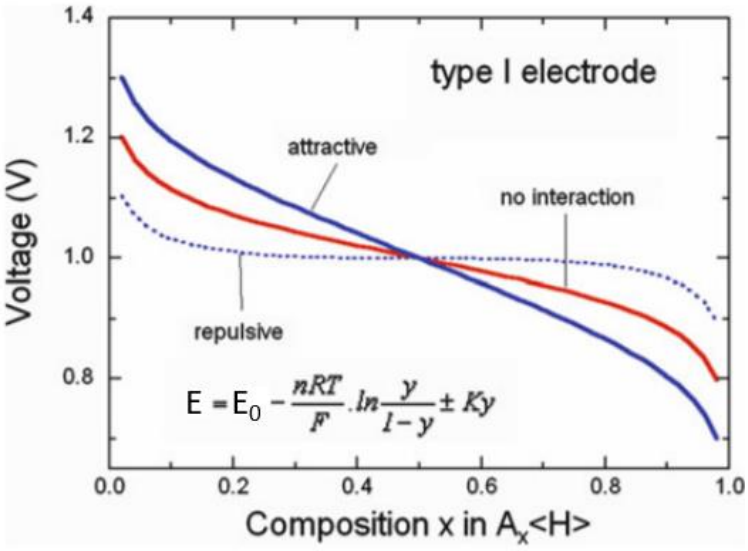

Figure 7: Voltage characteristic in ideal circumstances for batteries with insertion/intercalation mechanisms. The value of X is equal to the value of y [28]

To illustrate a voltage calculation, we use the system given in Figure 1.

$Cu^{2+} + 2\ e^- \rightarrow Cu$ +0.34 V (reduction)

$Zn^{2+} + 2\ e^- \rightarrow Zn$ -0.76 V (oxidation)

E_0 = reduction potential – oxidation potential = 0.34 V – (-0.76V) = 1.1 V

At a temperature of 20°C (293K) and a concentration of 0.5M oxidant and 0.1M reductant and no interactions between particles (meaning K=0). In the Nernst equation that gives:

$$E = 1.1V - \frac{8.314\frac{j}{mol*k}*293K}{2*96485\frac{A}{mol}}*\ln\left(\frac{0.5}{0.1}\right) = 1.08V$$

9.6.2 Battery capacity

Every active material has a specific capacity (C) expressed in Ampère hour per gram. It is calculated via eq. 2 . When considering the battery as whole, the capacity is expressed in Ampère hour or Coulomb. However, in order to consider the capacity of the battery, it is necessary to determine the specific capacity of the electroactive material's system. To calculate the specific theoretical capacity of the system, the sum of the inverted specific capacity of the two active materials has to be made. The inversion of this sum is the specific theoretical capacity of the battery. [29]

$$c = \frac{F*n}{M*3600} \quad (2)$$

As an example, the specific capacity of the copper/zinc cell is calculated.
The specific capacity of copper is:

$$c = \frac{96485 \frac{A}{mol} * 2}{63.54 \frac{g}{mol} * 3600} = 0.844 \text{ Ah/g}$$

The same calculation gives a theoretical capacity of 0.82 Ah/g for zinc. Now the specific capacity of the system is calculated:

$$c = (\frac{1}{0.82 \frac{Ah}{g}} + \frac{1}{0.844\ Ah/g})^{-1} = (2.42 \frac{g}{Ah})^{-1} = 0.416 \frac{Ah}{g}$$

9.6.3 Specific energy

With regard to the battery's specific energy (Wh/kg), it is important to make a distinction between the theoretical specific energy, which can simply be calculated via the multiplication of the theoretical cell voltage and the capacity of the battery, and the real specific energy of the battery. There are numerous factors contributing to the decrease of the battery's energy in comparison with the theoretical one. The first one is that the battery has certain components that are not electrochemically active but do contribute to the weight, like a separator and electrolyte. A second reason is that the electroactive chemicals are never present at stoichiometric quantities; there is always one in excess that causes the weight of the battery to increase. Another related cause is that electro-active materials never fully convert; there always remains a small quantity of product that is not reacting. The last reason is that batteries never discharge at theoretical voltage. This is due to the presence of polarizations.

Instead of looking at the mass of the electro-active components, calculations can also be made using the volume of the components. In that case the specific energy is replaced by energy density expressed in Watt-hour per litre.

9.6.4 Closed circuit voltage

When the battery is coupled with a load, a closed circuit is created and a current starts to flow. The voltage over this load is not equal to the theoretical voltage of the battery. Several effects, related to the current, cause the external voltage to drop and thus lower the rate capability of the cell. The current flowing in the circuit is related to the load; the lower the resistance of the load, the higher the current, the worst the battery performance. The three effects influencing the battery voltage are visualised in Figure 8.

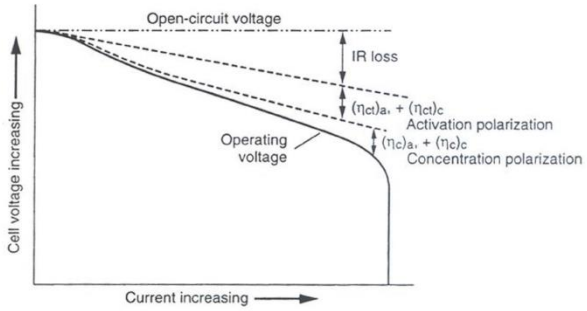

Figure 8. Battery voltage in function of current

9.6.5 Cut-off voltage

The cut-off voltage, is the voltage on which the battery is considered to be fully discharged. This is not the point where all the chemical energy is converted to electrical energy, but discharging beyond the cut-off voltage would result in remaining damage of the battery. Figure 9 shows the discharge curve of a LAB. As can be observed, can the battery discharge beyond the cut-off voltage. This is the deep discharge region in Figure 9. For a LAB, a discharge beyond the cut-off voltage causes strain and each discharge/charge cycle permanently robs the lead-acid battery of a small amount of capacity [25].

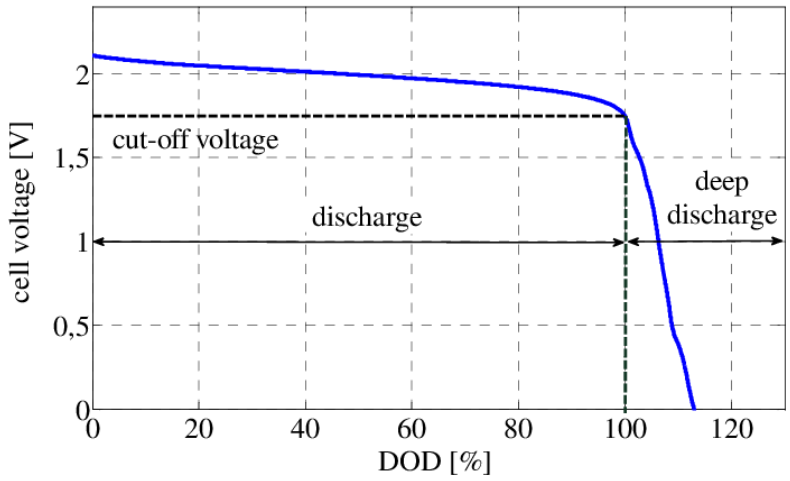

Figure 9. Discharge curve of a lead-acid battery [30]

9.7 BATTERY TERMINOLOGIES

9.7.1 Activation polarization

An electrochemical reaction proceeds in several steps. The slowest step is the rate determining step. For the electrochemical reaction to occur, the energy barrier of the rate determining step needs to be surmounted. This activation energy needed to start the reaction is a loss of useful energy. The activation losses are insensitive to the current and thus cause the constant voltage to drops.

9.7.2 Concentration polarization

Concentration polarization is a consequence of the reaction rate being controlled by diffusion of active species to the electrode. It manifests itself more clearly at high current densities (A/cm^2). The higher the current in a battery, the bigger the amount of ions present around the electrodes. The ion accumulation at the electrodes results in the formation of a diffusion layer. From this layer ions have the tendency to diffuse away from the electrode and thereby cause a potential gap. Resulting in voltage drop in the battery [6].

9.7.3 Ohmic polarization

A battery has many internal parts where the current needs to pass through, each of them having its own resistance. Those resistances cause ohmic drops in batteries, resulting in the electrical energy being internally converted to heat (Joule effect).

9.7.4 C-rate

The discharge and charge current is for batteries often expressed in terms of C-rate. The C-rate describes the current in relation with the total capacity of the battery. A 1C rate equals a total discharging time of one hour for a fully charged battery. For a battery with a capacity of 200 mAh this equals a discharging current of 200 mA. If the C-rate is 5C the current also multiplies by five and becomes 1 A [31].

9.7.5 Electrical double layer

By submerging a charged electrode in electrolyte, it attracts particles. Take an aqueous electrolyte in a negatively charged electrode as an example. Because water molecules are bipolar, the majority of them will place themselves with the positive pole towards the electrode. Let us assume a cation wants to approach the electrode. In most cases the cation would be well solvated and thereby have a sheet of water molecules surrounding it. These cations are not able to contact adsorb at the surface of the electrode but will have a minimal approachable distance. The imaginary plane that can be drawn around the electrode's minimal approachable distance is called the outer Helmholtz plane. Some large ions, like cesium ions, that do not solve well, can contact adsorb on the electrode. The distance they can approach the electrode to, is the same as the solvent molecules. This distance forms the inter Helmholtz plane. Figure 10 shows the planes for a positive electrode.

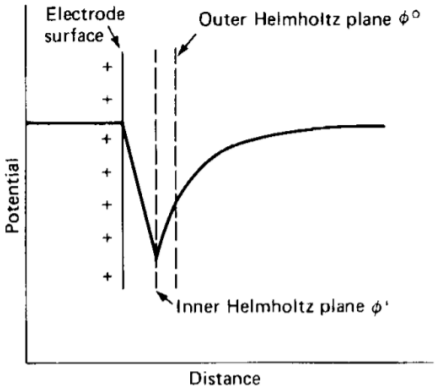

Figure 10. Charge distribution over the electrical double layer [29]

The charged surface of the electrode and the charged layer caused by the orientation of the solvent molecules, form together the so-called electrical double layer. The existence of the double layer has some consequences on the electron transfer. This will become more evident in Electrochemical impedance spectroscopy (EIS). Charge transfer reactions can best be described by the concentration of the electroactive species at the electrode, which is not the same as in the bulk. This is because the potential near the electrode differs from the potential in the bulk, which causes differences in concentrations. The concentration at the closest possible approachable distance is described by eq. 3.

$$C^e = C^b * e^{\frac{-n*F*\phi^e}{R*T}} \quad (3)$$

The double layer causes the rise of an impedance. It behaves like a capacitor in which the solvent molecules on the inner Helmholtz plane act like a dielectric. It separates the charged electrode from the solvated ions outside the Helmholtz plane. This in itself is the structure of a capacitor and therefore it acts like one. The presence of a capacity at the electrode surface influences the electron transfer.

9.8 ZINC BATTERIES

Zinc batteries have been used since the 19th century, from the moment Lechlanché introduced his electrochemical cell. The cell Lechlanché introduced and all of its successors were primary batteries. They use zinc as anode and mostly manganese dioxide as cathode. In these cells, the cathode reaction is the conversion of MnO_2 to MnOOH, in which Mn(IV) reduces to Mn(III). Simultaneously, Zn oxidizes to Zn^{2+}.

The batteries that nowadays are being used as secondary batteries for portable devices are lithium-ion batteries because of their high cyclability and high energy density. However, these batteries suffer from high safety risks: the used lithium is dangerous, and the batteries are flammable because of their organic electrolyte. This resulted in a series of incidents in 2016 when smartphone batteries of the new “Samsung Galaxy note 7” ignited [32]. Another problem for lithium-ion batteries is the rarity of lithium in the earth’s crust. It is only the 33th most common element, making lithium more and more difficult to gather at a low price. As a result, researchers are considering zinc, which is 3.5 times more common in the earth’s crust, as viable alternative for lithium secondary batteries [33].

Secondary zinc-ion batteries are still being developed gradually to become a viable replacement for lithium-ion batteries. The most important reason they aren’t yet, is their bad cyclability. In order for zinc-ion batteries to have good cycling stability, the intercalation reaction of zinc needs to be the main redox reaction. This makes the choice of a good cathode material vital. At this moment, three main types of cathode material have been proposed that have shown promising cycling performances: Prussian blue analogues, Vanadium-based oxides and manganese-based oxides [34]. This literature study will focus on different forms of manganese oxides.

9.8.1 Manganese dioxide cathodes

Manganese is the 12th most common element on earth, making it cheap and therefore a suitable cathode material. Manganese dioxide has proven to be the most promising candidate as cathode material, even though there are some auspicious studies using Mn_2O_3. [34] When considering manganese dioxide, the first thing that needs to be mentioned is the fact that there are multiple lattice structures of it. MnO_2 forms an octahedral structure (MnO_6) as seen in Figure 11. These octahedrons can arrange themselves in different ways, leading to the formation of different spatial structures. These can be seen in Figure 12, all of these structures have different electrical reaction mechanisms and characteristics.

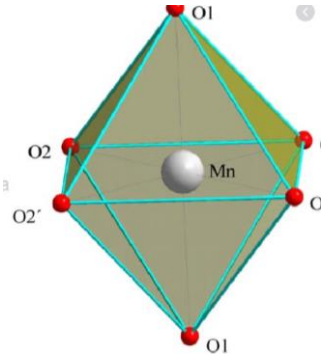

Figure 11. Octahedral structure of manganese dioxide [36]

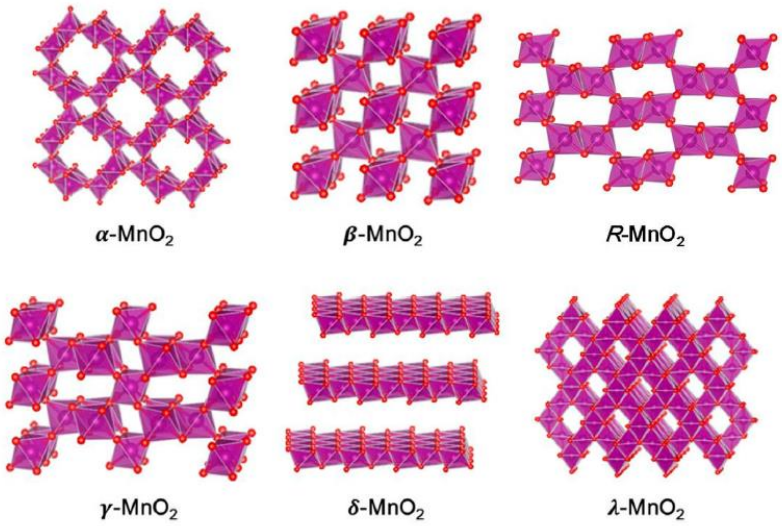

Figure 12. Polymorphs of manganese dioxide [37]

9.8.1.1 α-MnO_2

α-MnO_2 is a 2x2 tunnel structure of MnO_2, which means the octahedrons form a porous tunnel structure with each pore having a width of two octahedrons in the vertical and horizontal directions. This is the most studied structure for battery applications out of all the manganese oxide types. However, there is still a debate going on in the scientific community to accurately describe the reaction mechanism of α-MnO_2 as cathode in zinc batteries.

A first proposal is stated by Kim et al. It had been proven that $ZnMn_2O_4$ formed during discharge. They raised the possibility that the formation of $ZnMn_2O_4$ took place in two steps. This means that first one electron reduces one manganese atom, leading to the formation of $ZnMn_4O_8$. In a second stage of discharge, $ZnMn_2O_4$ is formed [38]. However, at this point there is insufficient evidence to support this theory.

$Zn^{2+} + 2\ e^- + MnO_2 \rightarrow ZnMn_2O_4$

A second reaction that occurs is the phase transformation of α-MnO_2. It is estimated that about one-third of the α-MnO_2 converts reversibly to birnessite (δ-MnO_2). A theory for the mechanism was put forward by Lee et al. [39] They claim that a phase-transformation takes place from α-MnO_2 to zinc intercalated buserite (buserite is birnessite with a bigger interlayer distance, 10 Å instead of 7 Å) [40]. The buserite then continuously transforms further to birnessite.

A third reaction that occurs at full discharge is the conversion reaction to $Zn_4(OH)_6SO_4\_nH_2O$ (ZHS). The reaction mechanism for this product is also unknown. Several different mechanisms have been proposed but none of them has been confirmed [34].

9.8.1.2 β-MnO_2

β-MnO_2 is the 1x1 tunnel structure of MnO_2. It is known to be the most stable polymorph of MnO_2 but at the same time, it has one of the lowest specific capacities due to the small tunnels that are hard to penetrate for ions. Zhang et al reported a reversible zinc storage mechanism in this structure [41].

The mechanism was observed in a mild acid environment with $Zn(CF_3SO_3)_2$ $Mn(CF_3SO_3)_2$ as electrolyte. In a first discharge cycle, one dominating reaction at 1.06V is observed, which is the result of a phase transition. The β-MnO_2 forms, in the same way as with α-MnO_2, MnO_2-buserite which intercalates Zn-ions at a high occupation. In subsequent charge/discharge cycles Zn insertion/extraction processes are observed but no phase transformations anymore. On X-ray pattern β-MnO_2 peaks fade away after some cycles. This leads to the belief that the phase transformation is irreversible.

Zhang et al demonstrated this reaction mechanism by using a nanorods structures. Apart from describing the storage mechanism, they were also able to perform some tests with the nanorods as cathode material. They measured a specific capacity of 135 mAh/g for the nanorods cathode, which is much higher than can be expected for β-MnO_2 at 6.5C. An important reason for the high capacity is the transformation to buserite. Furthermore, a good reversibility was shown for this cathode material, with only a 6% decline in capacity in 2000 cycles.

9.8.1.3 R-MnO_2

R-MnO_2, also referred to as ramsdellite, is a polymorph of manganese dioxide with a 2x1 tunnel structure. Wilkinson et al reported a specific capacity of 200 mAh/g at a c/15 c-rate. [42] After 1000 cycles the cathode is able to retain 65% of its original capacity. The mechanism

is described for the first discharge cycle. It is a two phase reaction mechanism, where formation of buserite, todorokite (3x3 tunnel structured MnO_2) and tetragonal spinels (Figure 13) takes place. The following cycles the electrochemical cathode reaction is described as a combination of those phase transformations and other, yet unknown zinc-containing reactions. The precise mechanism is still unknown for this species.

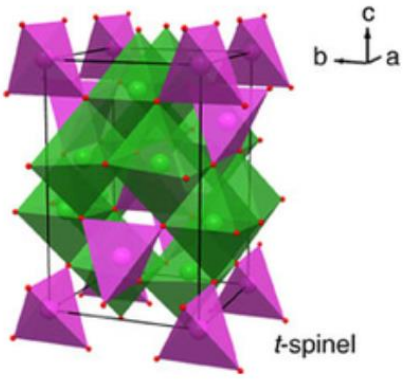

Figure 13. Tetragonal spinel structure [43]

9.8.1.4 δ-MnO_2

Contrary to the other structures discussed so far, δ-MnO_2 forms a layered structure of manganese dioxide octahedrons. The space between the layered structures (interlayer) is mostly filled with solvated ions. Ming et al reported that; "because of the (de)intercalation-type storage mechanism of ZIBs, layered electrode materials are generally preferable, and materials with large layer spacings are expected to possess good performance." [44]. It is known that δ-MnO_2 has the highest capacity of all the different forms of MnO_2 [45].

In contrast to this upside, δ-MnO_2 has several properties causing it to have bad cyclability performances. The first property is phase transformation: when discharged substances like ZnO, MnO and MnOOH are formed, the total volume may change, resulting in capacity decay. This is caused by the active material desquamating and thus disconnecting from the electrode.

A second problem of birnessite is its structural instability [46]. During the first discharge cycle, the interlayers are being filled with electroactive ions as a result of diffusion and intercalation. When thereafter the battery is discharged, the intercalated ions diffuse away from the interlayers, causing the layer structure to collapse.

Huang et al successfully created a structure of birnessite that was reinforced with polyaniline. The polyaniline served in the interlayers as pillars that on one hand prevented the structure to collapse, and on the other hand prevented phase transformation to occur. Huang at al reported promising results with a high cycle life stability of 40% (of the theoretical capacity of MnO_2, being 308 mAh/g) at high currents of 2A/g [47].

9.8.1.5 γ-MnO_2

The reaction mechanism occurring is highly dependent on numerous factors such as the current density, electrolyte, etc. However, Chabre et al [48] outlined the general reaction

events happening. Firstly, a homogeneous reaction occurs, during which protons intercalate between the γ-MnO_2 structure. This reaction is shown to be highly reversible, yet only occurs when the depth of discharge is 10% or lower. This means that only 10% of the total capacity has been discharged. In a second phase, a heterogeneous reaction starts, accompanied by a phase transformation. γ-MnO_2 forms two different phases, namely $Mn(OH)_2$ and Mn(OOH).

The discharge reaction with the formation of Mn(OOH) is important. It forms the main reason for the irreversibility of the Zn/γ-MnO_2 batteries. During the discharge, α-Mn(OOH) and γ-Mn(OOH) are formed out of MnO_2. This is the first reaction step, corresponding with the first electron reduction. The second electron reduction causes the formation of $Mn(OH)_2$ and Mn_3O_4. The Mn_3O_4 is a poor electrical conductor, leading to capacity fading. It only partially converts back to $Mn(OH)_2$, which means that it remains in the battery and grows in quantity every cycle, leading to a fast capacity decrease. The continuous discharge reaction figures in Figure 14.

An important note to make is that zinc also forms an irreversible product, namely $ZnMn_2O_4$. The formation occurs as follows:

$$2\ Mn(OOH) + Zn(OH)_4^{2-} \rightarrow ZnMn_2O_4 + 2\ H_2O + 2\ OH^-$$

Hertzberg et al did not include this into Figure 14 because this is not an electrochemical reaction (the oxidation number of the elements does not change). This reaction is mainly dominant in alkaline batteries. The higher the OH^-concentration, the more $Zn(OH)_4^{2-}$ is formed.

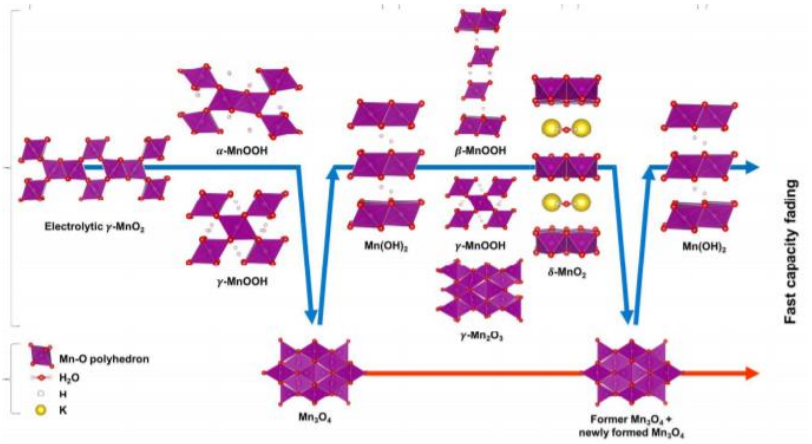

Figure 14. Reaction mechanism of γ-MnO_2 during discharge [49]

9.8.1.6 λ-MnO_2

λ-MnO_2 has a cubic spinel structure as can be seen in Figure 12 . Yuan et al have reported a specific capacity around 150 mAh/g at a current density of 68 mA/g. However, at high current densities of 408 mA/g the observed capacity decreased drastically to 33.8mAh/g. The observed mechanism was anticipated to be a zinc-intercalation mechanism similar to the intercalation mechanism in lithium batteries [50].

9.8.1.7 ε-MnO_2

Zhao et al [37] described this structure as "a metastable phase composed of face-shared [MnO_6] and [YO_6] octahedral (Y means vacancy), where Mn^{4+} cations randomly occupy 50% of the octahedral positions of the hexagonal-close packed (hcp) oxygen sublattice." Wei et al have been able to construct a ε-MnO_2 nanocrystal cathode in a mildly acidic aqueous electrolyte solution. They argued that the dissolution process of Mn^{2+} is a major reason for capacity fading in the battery and, by adding Mn^{2+} to the electrolyte as well as using nanocrystals constructed via the in situ electrodeposition method on carbon fiber paper, they were able to counter these effects. The dissolved manganese ions were electro-oxidized back on the cathode when the battery was recharged. The cycling performance of these cathodes is therefore promising. Zhao et al reported two insertion reactions. The first to occur is the intercalation of the H^+ ions. The second is the intercalation of the Zn^{2+} ions [51].

9.9 DOPING CATHODE MATERIAL

Doping has been proposed as a method to increase cathode quality, more specifically lowering resistance and raising the capacity. Wang et al [52] experimented by doping a manganese dioxide film with silver. The capacitance raised from 400 to 760 F/g at a scan-rate of 2mV/s. The mass in the films was 50 μg/cm². Results with higher masses of manganese dioxide were even more significant. For a mass of 160μg/cm², the capacities of the undoped and doped sample were respectively 8 and 147 F/g. The author indicated that the big difference was a result of the difference in resistance. This is supported by the results of the EIS. Qin et al [53] used boron as non-metallic doping material for MnO_2. The boron doped samples reached a capacitance of 269 F/g whereas the undoped sample had a capacitance of 206.4 F/g at a discharge speed of 50 mV/s. Raheem et al doped γ-MnO_2 with copper and iron. They showed that both iron and copper doped samples had a decrease in charge transfer resistance. Between those two, the decrease in resistance was the lowest for the copper doped sample. Raheem et al [9] speculated that because copper is more conductive it decreased the resistance more. Finally Liu et al [54] synthesized vanadium doped δ-MnO_2. The vanadium also deposited in the interlayers, resulting in smaller interlayer distances. The charge transfer resistance almost was halved at a mass percentage of 5% vanadium.

9.10 ANALYSIS TECHNIQUES

9.10.1 Cyclic voltammetry (CV)

A CV-test is an analysis method in which a voltage, applied on a working electrode, is changing at a constant rate to a maximum voltage and then changes back at the same rate to the start voltage. The current resulting of the imposed voltage is then plotted in function of that voltage. This voltage cycling can be repeated multiple times in a row. The plots give information about the stability of the electroactive components. They also indicate the presence of side reactions and show the reversibility of the charge discharge proces.

The setup and parameters of a CV-test are important. First of all, it is important to know the three different electrodes that are required, as well as their function. The working electrode is the electrode where the electrochemical proces that is investigated occurs. Because of the necessity for a closed circuit, a second electrode is used, this is the counter electrode. The third and last electrode that is used is the reference electrode. The potential on the working electrode is measured relative to this electrode. The most commonly used reference electrode is the silver/silver chloride electrode.

Besides the electrodes, another important factor is the scan rate, which has an impact on the height of the peak current. The relation for a reversible system is given by the Randles-Sevcik equation (eq. 4). The place of the peak and the peak potential, is for reversible systems not determined by the scan rate. A last important influence the scan rate has, is on the reversibility of the system. A system can behave reversibly at a low scan rate but become quasi-reversible or even irriversible at high scan rates. This becomes evident when testing at different scan rates and observing shifts of peak voltages.

$$I_p = (2{,}69 * 10^5) * \ n^{3/2} * A * D_j^{1/2} \ * C^e * v^{1/2} \tag{4}$$

In order to understand the results of a CV-test, it is important to understand the shape of the CV-test graph. In Figure 15 H, a typical curve of a CV-test is drawn. In the first stage (starting from A) a negligible current, called the charging current, is flowing. This current is present because of the double layer capacity, but it is almost zero and therefore not relevant to the test. At a certain voltage, in Figure 15 0.1V, a current starts to flow. This is due to a reaction occurring at the electrode surface. The current can be derived from the concentration profiles near the surface of the electrodes. The slope of the tangent of those profiles at place zero (against the electrode surface) determines the current. Figure 15 A-C shows that the concentration of the oxidant decreases, the amount with which it is decreasing can be explained by the Nernst equation. The lower the voltage, the lower the oxidant concentration.

The current reaches its maximum when the slope of the tangent has reached its maximum. Beyond the maximum, at a certain moment, the concentration of oxidant reaches zero at the electrode surface. At this moment, the current follows the Cottrell equation (eq. 5). This is valid as long as the oxidant concentration at the surface remains zero. An important aspect to highlight is that, at that moment, the current changes independently from the applied voltage.

$$i = \frac{n*F*A*c_j^0*\sqrt{D_j}}{\sqrt{t*\pi}} \tag{5}$$

When the scan rate is reversed at the set point, the reduction reaction keeps happening until the current starts increasing in the other direction. At this moment, the oxidation of the formed product starts. Here the same rules as before apply: the amperage is dependent on the slope of the tangent of the concentration profile at the electrode surface, and both the conditions for a maximum as well as the point of applicability for the Cottrell equation are the same.

An important parameter that can be learned from cyclic voltammetry tests is the formal potential, which can be a good approximation for the standard potential. The formal potential

is reached when the oxidant and reductant concentrations near the electrode surface are equal (Figure 15 point B and E). This can be derived from the Nernst equation (eq. 1), when a_{red} equals a_{ox}, the potential is equal to the formal potential. A description on how to derive the formal potential from CV graphs is given by Elgrishi et al [22].

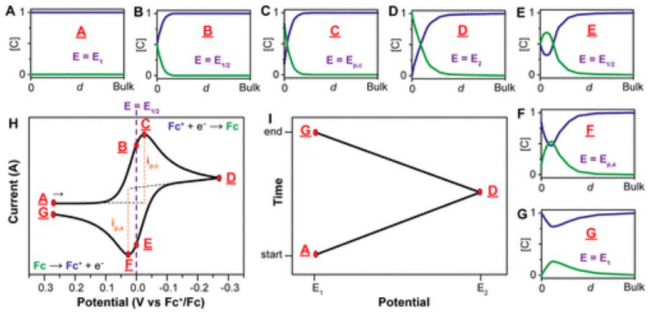

Figure 15. (A-G) Concentration profiles during CV-test, where x=0 is the electrode surface, the green line is the reductant concentration and the blue line the oxidant concentration. (H) the corresponding CV-graph. (I) the applied voltage in function of the time [22]

The reversibility can be derived if the amount of electrons participating in the electrochemical reaction is known. A perfect reversible system has a peak separation of 0.059/n V. The further the peaks are separated, the more irreversible the system is. If the backwards scan does not have a peak, the system is referred to as irreversible. If apart from the expected peak, second peaks occur, it can indicate that there are multiple electrochemical reactions or that there are adsorbed species at the electrode surface. Finally, the stability of the electrochemical products can be derived from the decrease of peak area between different cycles.

9.10.2 Electrochemical impedance spectroscopy (EIS)

With this technique, the impedance of the battery is measured via an imposed AC signal. This allows for the determination of the impedance over a wide frequency range. The impedance is always expressed in a real part (Z') and an imaginary part (Z''), these two parts are plotted against each other (Nyquist plot). From this plot different parameters can be derived. The most standard used model for batteries is shown in

Figure 16. It contains the resistance R_s, which stands for the resistance of the electrolyte material. It also contains R_{ct}, which is the charge transfer resistance. Then there is C_{dl}, this is the capacity created by the electrical double layer (see Electrical double layer). And finally, there is the Warburg impedance W [55]. The Warburg impedance gives the diffusion effects of the active species and can therefore be divided into two terms: a term for the reductant and a term for the oxidant. In order for this model to be a good approximation for a real battery, the EIS test must be executed around equilibrium and the amplitude of the AC signal must be kept small.

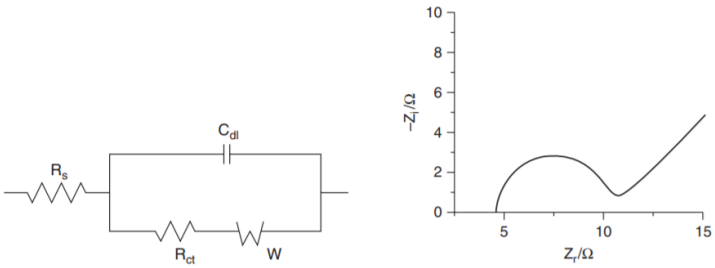

Figure 16. Randles' equivalent circuit for an electrode/electrolyte interface including the Warburg impedance and the corresponding Nyquist plot [55]

9.10.3 X-ray diffraction

X-ray diffraction (XRD) is an analysis method that is used to determine the lattice-structure of a crystalline substance. The technique uses X-rays and fires them on the surface of a sample. The X-rays then excite some electrons whose energy state rises because of the X-ray absorption. In order to lose the energy, the electrons re-emit the radiation. This process is called elastic scattering. The broadcast of the re-emitted radiation occurs in all directions. A sensor of the apparatus will measure the intensity of the incoming radiation.

The distance of the atoms causes the broadcasted radiation to interfere constructively in some angles. The sensor of the apparatus scans the radiation thus under a continuum of angles. The intensity will then be plotted versus the angle of measurement (2θ). In Figure 17 the meaning of the angle 2θ is illustrated. Out of the interference angles, the distances between the atoms/molecules can be learned. However, in most cases researchers just compare their XRD-graphs with already existing graphs to check the lattice-structure.

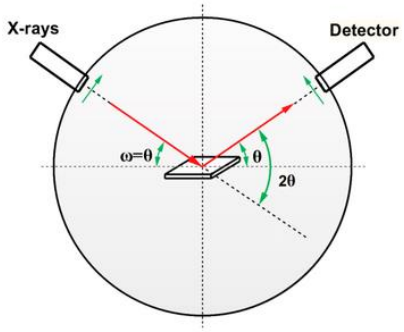

Figure 17. Analysis of sample in an XRD [56]

9.10.4 Scanning electron microscopy (SEM)

SEM is a microscopic technique that allows researchers to create three dimensional enlarged images with a maximum spatial resolution of 50 nm [57]. The technique uses energetic electron beams that it fires on a sample. The electrons than interfere with the samples surface, these interferences result in the emission of other electrons that are used for imaging. SEM is well liked because it is non-destructive and is able to produce high resolution images.

10 EXPERIMENTAL METHOD

10.1 SYNTHESIS

The synthesis section includes two parts. The first one describes the synthesis of undoped and Cu-doped birnessite. The second part explains the fabrication of the cathode containing birnessite.

10.1.1 Part one: Synthesis of δ-MnO_2 and Cu-doped-δ-MnO_2

The method to synthesise birnessite is described by Schubert et al. [10]

The first step is the chemical reaction to create poor crystalline birnessite at room temperature. 50ml of a 0.3M $Mn(NO_3)_2.6H_2O$ solution was heavily stirred. This was followed by the addition of 50ml solution of 10V% H_2O_2 and 0.6M NaOH. Now an exothermic reaction would occur leading to black precipitation. After the reaction, the precipitation was stored statically for 12h. The obtained precipitation was the poor crystalline birnessite. For the preparation of doped birnessite 0.015M $CuSO_4$ was added to the manganese solution. The formed birnessite was washed with 100ml distilled water three times. Thereafter the birnessite was put in a vacuum oven at 60°C for 16h.

In the second step, 1g of the formed birnessite was put in an autoclave reactor with 15ml of a 1M NaOH solution. Next, the autoclave was placed in an oven. The hydrothermal temperature was maintained at 150°C for 12h. Then, highly crystalline birnessite was formed with Na^+ ions in the interlayers. To exchange the sodium ions, an ion exchange was performed. The resultant birnessite precipitant was immersed in a bath containing 1M $Zn(NO_3)_2$. 12h later, it was washed 3 times with 100ml distilled water. Finally, the sample was collected and dried again in a vacuum oven at 60°C for 16 h, resulting in a powdery sample of (Cu-doped) δ-MnO_2.

10.1.2 Part two: Fabrication of cathodes

To investigate the electrochemical properties of δ-MnO_2 before and after doping Cu, the MnO_2 cathodes were prepared using a paint coating method. In particular, 45mg of the cathode material was mixed with 45mg of super carbon P, which serves as conductive agent, and 10mg of polyvinylidene fluoride (PVDF), which serves as binder. The mixture was then pulverized, using a mortar and pestle for 30 minutes. After that, about 200 µl of N-Methyl-2-pyrrolidone (NMP) solvent was added to form a black slurry like paint. Finally, the cathode paint was coated to a thin layer on the surface of a Ni foam with a diameter of 2cm. Finally, the electrodes were dried in a vacuum oven for 12h at 80°C.

10.2 STRUCTURAL CHARACTERISATION

10.2.1 XRD

To characterize phase structure of synthesized MnO_2 materials, XRD method was used. The powdery samples were analysed using XRD with a 2θ range of 10÷80° and a scan rate of 3°/min. Expected results for birnessite XRD patterns are shown in Figure 18.

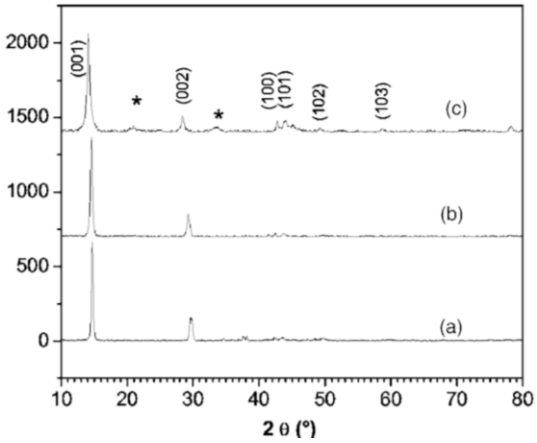

Figure 18. XRD patterns of δ-MnO2 [58]

10.2.2 SEM

This test uses the synthesised powdery sample that is created at the end of "Part one: Synthesis of δ-MnO2 and Cu-doped-δ-MnO2". The sample is send to an external lab and the images get delivered back. The test is used after the XRD as an extra conformation technique to verify the formed structure and gather more information about the structure, especially, the interlayer distance of the birnessite.

10.3 ELECTROCHEMICAL CHARACTERISATIONS

To implement electrochemical measurements, a zinc-ion battery (cell) was assembled. In detail, a CR2032-coin-type zinc-ion cell was constructed by using a Zn metal foil as anode, a MnO_2 cathode and a separator which was impregnated with 300 μl of an aqueous solution containing 1M $ZnSO_4$ and 1M $MnSO_4$ The image of an assembled zinc-ion cell is presented in Figure 19.

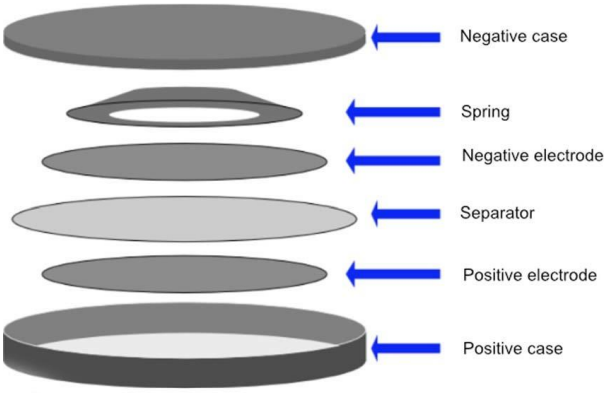

Figure 19. CR2032-coin-type cell [59]

10.3.1 CV

The CV-graph of birnessite should look like Figure 20. Firstly, to investigate the intercalation and deintercalation of Zn^{2+}, CV method was employed. The measurement was conducted between a potential of 1.0 and 1.8V. A scan rate of the CV measurement was fixed at 0.1 mV/s

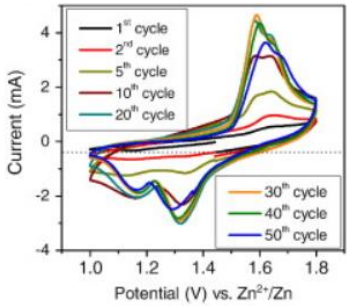

Figure 20: CV-graph of birnessite [60]

10.3.2 EIS

EIS is a powerful method to evaluate the parameters impacting the redox mechanism of any electrode active material. In the present work, EIS method was also used to examine the effect of doping Cu into δ-MnO_2 material on its electrochemical performance. EIS measurements were carried out at the frequency from 100mHz to 10kHz with an amplitude of 5mV. All measurements were executed at room temperature.

11 REFERENCES

[1] W. Xu en i. Wang, „Recent Progress on Zinc-Ion Rechargeable Batteries," *Nano-Micro Letters,* vol. 2019, nr. 11, 2019.

[2] M. H. Alfaruqi, J. Gim, S. Kim, J. Song en D. T. Pham, „A layered δ-MnO2 nanoflake cathode with high zinc-storage capacities for," *electrochemistry communications,* vol. 2015, nr. 60, pp. 121-125, 2015.

[3] M. Song, H. Tan, D. Chao en H. J. Fan, „Recent Advances in Zn-Ion Batteries," *Advanced functional materials,* vol. 2018, nr. 28, 2018.

[4] W. Lu, C. Xie en H. Zhang, „Zinc dendrites Inhibition for Zinc-based Battery," *chemsuschem,* vol. 2018, nr. 11, p. 23, 2018.

[5] Z. Zhao, Z. J, Z. Hu, L. J, J. Li, Z. Y en C. Wang, „Long-life and Deeply Rechargeable Aqueous Zn Anodes Enabled by Multifunctional Brightener-Inspired Interphase," *Energy & environmentel science,* vol. 2019, nr. 6, p. 12, 2019.

[6] D. Kopeliovich, „Substech," 31 05 2012. [Online]. Available: https://www.substech.com/dokuwiki/doku.php?id=polarization.

[7] C. Liu, Y. Chen, Z. D. Xiao, j. Wu, Y. Situ en H. Huang, „Tuning Mn2+ additive in the aqueous electrolyte for enhanced cycling stability of birnessite electrodes," *electrochimica acta,* vol. 2019, nr. 298, pp. 678-684, 2019.

[8] L. Liu, Q. Feng, K. Yanagisawa, G. Bignall en T. Hashida, „Lithiation reactions of Zn- and Li-birnessites in non-aqueous solutions and their stabilities," *journal of material science,* vol. 2002, nr. 37, pp. 1315-1320, 2002.

[9] Z. H. Raheem en A. M. A. Alsammarraie, „Hydrothermal synthesis of γ-MnO2 star shape nanostructures and the effect of doping with (Fe and Cu) on their electrochemical performance in zinc-MnO2 rechargeable batteries.," *Research Journal of Pharmaceutical, Biological and Chemical ,* vol. 2018, nr. 9, pp. 1450-1458, 2018.

[10] U. Schubert, N. Hüsing en R. Laine, „Birnessite-type Manganese Oxide by Redox Precipitation," in *Material synthesis a practical guide*, New York, Springer NewYork, 2008, pp. 65-68.

[11] M. Feng, Q. Du, L. Su, G. Zhang, G. Wang en Z. Ma, „Manganese oxide electrode with excellent electrochemical performance for sodium ion batteries by pre-intercalation of K and Na ions," *scientific reports,* 2017.

[12] S. Ching, D. Petrivay en M. Jorgensen, „Sol−Gel Synthesis of Layered Birnessite-Type Manganese Oxides," *Inorganic Chemistry,* vol. 1997, nr. 36, pp. 883-890, 1997.

[13] „Palmsens," 2020. [Online]. Available: https://www.palmsenscorrosion.com/knowledgebase/electrochemical-impedance-spectroscopy/. [Geopend 02 26 2020].

[14] N. Qui, H. Chen, Z. Yang, S. Sun en Y. Wang, „Low-cost birnessite as a promising cathode for high-performance aqueous rechargeable batteries," *Electrochimica Acta,* vol. 2018, nr. 272, pp. 154-160, 2018.

[15] Wikipedia, „Wikipedia," 2019. [Online]. Available: https://en.wikipedia.org/wiki/Electrochemical_cell#/media/File:Galvanic_cell_with_no_cation_flow.svg. [Geopend 05 May 2020].

[16] Gillard, „Illustration d'une pile de Volta," *Leçons de Physique,* nr. Vuibert et Nony, 1904.

[17] B. J. Lossing, „Trough battery," Cassel & company, Londen, England, 1891.

[18] S. C. Rasmussen, History of Energy Technologies and Lessons for the Future, Firenze : Firenze University Press, 2019.

[19] B. J. Lossing, „Grove Cell," Cassel&Company, Londen, 1891.

[20] A. S. Dutton, J. M. Fukuto en K. N. Houk, „Theoretical Reduction Potentials for Nitrogen Oxides from CBS-QB3 Energetics and (C)PCM Solvation Calculations," *inorganic chemistry,* vol. 2005, nr. 44, pp. 4024-4028, 2005.

[21] P. Marsal, „Dry Cell". United States Patent 2605298, 29 July 1952.

[22] N. Elgrishi, K. J. Rountree, B. D. McCarthy, E. S. Rountree, T. T. Eisenhart en J. L. Dempsey, „A Practical Beginner's Guide to Cyclic Voltammetry," *Chemical education,* vol. 2018, nr. 95, pp. 197-206, 2018.

[23] J. e. al, „principles of intercalation," in *Lithium batteries*, Switzerland, Springer International Publishing, 2016, pp. 69-91.

[24] K. P., „Gaston Planté and his invention of the lead-acid battery-The genesis of the first practical rechargeable battery," *Journal of Power Sources,* vol. 2010, nr. 195, pp. 4424-4434, 2010.

[25] I. Buchman, „Battery university," 2020, [Online]. Available: https://batteryuniversity.com/learn/archive/can_the_lead_acid_battery_compete_in_modern_times. [Geopend 3 April 2020].

[26] D. T., „Li-ion and lead-acid battery applications push global battery materials market toward $43.2 bn by 2023," *Focus on catalyst,* p. 2, July 2018.

[27] HET EUROPEES PARLEMENT EN DE RAAD , „ batterijen en accu's, alsook afgedankte batterijen en accu's en tot intrekking van Richtlijn 91/157/EEG," Europese Unie, Straatsburg, 2006.

[28] C. Julien, A. Mauger, A. Vijh en K. Zaghib, „Principal of intercalation," in *Lithium batteries*, Switzerland, Springer, 2019, pp. 69-91.

[29] D. Linden en T. B. Reddy, Handbook of batteries, United States: McGraw-Hill, 2001.

[30] T. Blank, J. Badeda, J. Kowal en D. U. Sauer, „Deep Discharge Behavior of Lead-Acid Batteries and Modeling of Stationary Battery Energy Storage Systems," *International Telecommunications Energy Conference,* nr. 34, 2012.

[31] MIT Electric Vehicle Team, „A Guide to Understanding Battery Specifications," December 2008. [Online]. Available: http://web.mit.edu/evt/summary_battery_specifications.pdf. [Geopend 02 June 2020].

[32] H. Blankesteijn, „Galaxy Note 7 ontplofte van pure dunheid," *De ingenieur,* 9 December 2016.

[33] Lumen, „Reading: Abundance of Elements in Earth's Crust," Lumen, [Online]. Available: https://courses.lumenlearning.com/geology/chapter/reading-abundance-of-elements-in-earths-crust/. [Geopend 08 04 2020].

[34] Y. Zhao, Y. Zhu en X. Zhang, „Challenges and perspectives for manganese-based oxides for advanced aqueous zinc-ion batteries," *Wiley,* 2019.

[35] B. Jiang, C. Xu, C. Wu, L. Dong, J. Lia en F. Kang, „Manganese Sesquioxide as Cathode Material for Multivalent Zinc Ion Battery with High Capacity and Long Cycle Life," *Electrochiminica Acta,* vol. 2017, nr. 229, pp. 422-428, 2017.

[36] M. Tseggai, R. Mathieu en P. Nordblad, „Magnesium substitution in Nd 0.7Sr 0.3 MnO 3," *Journal of solid state chemistry,* vol. 2004, nr. 177, pp. 966-971, 2004.

[37] J. Shin, J. K. Seo, R. Yaylian, A. Huang en Y. S. Meng, „A review on mechanistic understanding of MnO2 in aqueous electrolyte for electrical energy storage systems," *International Materials Reviews,* 2019.

[38] M. H. Alfaruqi, J. Gim, S. Kim, J. Song, J. Jo, S. Kim, V. Mathew en J. Kim, „Enhanced reversible divalent zinc storage in a structurally stable α-MnO2 nanorod electrode," *Journal of Power Sources,* vol. 2015, nr. 288, pp. 320-327, 2015.

[39] B. Lee, H. R. Lee, H. Kim, K. Y. Chung, B. W. Choa en S. H. Oh, „Elucidating the intercalation mechanism of zinc ions into α-MnO2 for rechargeable zinc batteries," *Chemical Communications,* vol. 2015, nr. 51, pp. 9265-9268, 2015.

[40] A. Scheinost, „Metal oxides," in *Encyclopedia of Soils in the Environment*, columbia University, Reference module, 2005, pp. 428-438.

[41] N. Zhang, F. Cheng, J. Liu, L. Wang, X. Long, X. Liu, F. Li en J. Chen, „Rechargeable aqueous zinc-manganese dioxide batteries with high energy and power densities," *Nature communications,* 2017.

[42] I. Stoševski, A. Bonakdarpour, F. Cuadraa en D. P. Wilkinson, „Highly crystalline ramsdellite as a cathode material for near-neutral aqueous MnO2/Zn batteries," *Chemical communications,* vol. 2019, nr. 55, pp. 2082-2085, 2019.

[43] C. Li, X. Han, f. Cheng en Y. Hu, „Phase and Composition Controllable Synthesis of Cobalt Manganese Spinel Nanoparticles towards Efficient Oxygen Electrocatalysis," *Nature communications,* vol. 2015, 2015.

[44] F. Ming, H. Liang, Y. Lei, S. Kandambeth, M. Eddaoudi en H. N. Alshareef, „Layered MgxV2O5·nH2O as Cathode Material for High-Performance Aqueous Zinc Ion Batteries," *ACS energy Lett.,* vol. 2018, nr. 10, pp. 2602-2609, 2018.

[45] D. Selvakumaran, A. Pan, S. Liang, G. Cao en J. Mater, „A review on recent developments and challenges of cathode materials for rechargeable aqueous Zn-ion batteries," *Journal of Materials Chemistry A,* vol. 2018, nr. 6, pp. 4883-5230, 2018.

[46] 2. J. S. Y. W. Xian-Zhi Zhai1, Juan Wang, Wei Li, Yasmine Abdelkrim, Hongfu Yuan en Zhong-Zhen Yu, „Layered Birnessite Cathode with a Displacement/ Intercalation Mechanism for High-Performance Aqueous Zinc-Ion Batteries," *Nano-Micro Letters,* vol. 2020, 2020.

[47] J. Huang, Z. Wang, M. Hou, X. Dong, Y. Liu, Y. Wang en Y. Xia1, „Polyaniline-intercalated manganese dioxide nanolayers as a high-performance cathode material for an aqueous zinc-ion battery," *Nature communications,* vol. 2018, nr. 9, pp. 1-8, 2018.

[48] Y.Chabre en J.Pannetier, „Structural and electrochemical properties of the proton / γ-MnO2 system," *Progress in Solid State Chemistry,* vol. 1995, nr. 23, pp. 1-130, 1995.

[49] B. J. Hertzberg, A. Huang, A. Hsieh, M. Chamoun, G. Davies, J. K. Seo, Z. Zhong, C. Mark, E. Can, M. Y. Shirley en S. Dan, „The effect of multiple cation electrolyte mixtures on rechargeable Zn-MnO2 alkaline batteries," *Chemistry of materials,* 2016.

[50] C. Yuan, Y. Zhang, Y. Pan, X. Liu, G. Wang en D. Cao, „Investigation of the intercalation of polyvalent cations (Mg2+, Zn2+) into λ-MnO2 for rechargeable aqueous battery," *Electrochimica Acta,* vol. 2014, nr. 116, pp. 404-412, 2014.

[51] W. Sun, F. Wang, S. Hou, C. Yang, X. Fan, Z. Ma, T. Gao, F. Han, R. Hu, M. Zhu en C. Wang, „Zn/MnO2 Battery Chemistry With H+ and Zn2+ Coinsertion," *Journal of the American chemistry society,* vol. 2017, nr. 139, p. 9775−9778, 2017.

[52] Y. Wang en I. Zhitomirsky, „Cathodic electrodeposition of Ag-doped manganese dioxide films for electrodes of electrochemical supercapacitors," *Materials Letters,* vol. 2011, nr. 65, pp. 1759-1761, 2011.

[53] H. Z. Chi, Y. Li, Y. Xina en H. Qin, „Boron-doped manganese dioxide for supercapacitors," *Chemical communications,* vol. 2014, nr. 50, pp. 13349-13352 , 2014.

[54] L. Liu, M. Min, F. Liu, H. Yin, Y. Zhang en G. Qui, „Influence of vanadium doping on the supercapacitance performance of hexagonal birnessite," *Journal of power sources,* vol. 2015, nr. 277, pp. 26-35, 2015.

[55] T. B. Reddy, „EIS," in *handbook of batteries 4th edition*, New York, MCGraww Hill, 2011, pp. 2.25-2.28.

[56] M. Raza, „Oxygen vacancy stabilized zirconia (OVSZ); synthesis and properties,” 2017.

[57] S. Swapp, „Geochemical Instrumentation and Analysis,” Montana state university, 26 May 2017. [Online]. Available: https://serc.carleton.edu/research_education/geochemsheets/techniques/SEM.html. [Geopend 02 June 2020].

[58] T. Brousse, M. Toupin, R. Dugas en L. Athouël, „Crystalline MnO2 as Possible Alternatives to Amorphous Compounds in Electrochemical Supercapacitors,” *Journal of The Electrochemical Society,* vol. 2006, nr. 153, pp. 2171-2180, 2006.

[59] W. Kao-ian, R. Pornprasertsuk, P. Thamyongkit en T. Maiyalagan, „Rechargeable Zinc-Ion Battery Based on Choline Chloride-Urea Deep Eutectic Solvent,” *Journal of The Electrochemical Society,* vol. 6, nr. 166, pp. 1063-1069, 2019.

[60] M. H. Alfaruqi, J. Gim, S. Kim, J. Song, D. T. Pham, J. Jo, Z. Xiu, V. Mathew en J. Kim, „A layered δ-MnO2 nanoflake cathode with high zinc-storage capacities for eco-friendly battery applications,” *Electrochemistry communications,* nr. 60, pp. 121-125, 2015.

[61] University of texas, „Introduction to Electrochemistry,” University of Texas, 2013. [Online]. Available: http://ch302.cm.utexas.edu/echem/echem-all.php. [Geopend 28 03 2020].

12 APPENDIX

Reduction Half-Reaction		$E°$ (V)
$F_2(g) + 2\ e^-$	$\rightarrow 2\ F^-(aq)$	+2.87
$H_2O_2(aq) + 2\ H_3O^+(aq) + 2\ e^-$	$\rightarrow 4\ H_2O(\ell)$	+1.77
$PbO_2(s) + SO_4^{2-}(aq) + 4\ H_3O^+(aq) + 2\ e^-$	$\rightarrow PbSO_4(s) + 6\ H_2O(\ell)$	+1.685
$MnO_4^-(aq) + 8\ H_3O^+(aq) + 5\ e^-$	$\rightarrow Mn^{2+}(aq) + 12\ H_2O(\ell)$	+1.52
$Au^{3+}(aq) + 3\ e^-$	$\rightarrow Au(s)$	+1.50
$Cl_2(g) + 2\ e^-$	$\rightarrow 2\ Cl^-(aq)$	+1.360
$Cr_2O_7^{2-}(aq) + 14\ H_3O^+(aq) + 6\ e^-$	$\rightarrow 2\ Cr^{3+}(aq) + 21\ H_2O(\ell)$	+1.33
$O_2(g) + 4\ H_3O^+(aq) + 4\ e^-$	$\rightarrow 6\ H_2O(\ell)$	+1.229
$Br_2(\ell) + 2\ e^-$	$\rightarrow 2\ Br^-(aq)$	+1.08
$NO_3^-(aq) + 4\ H_3O^+(aq) + 3\ e^-$	$\rightarrow NO(g) + 6\ H_2O(\ell)$	+0.96
$OCl^-(aq) + H_2O(\ell) + 2\ e^-$	$\rightarrow Cl^-(aq) + 2\ OH^-(aq)$	+0.89
$Hg^{2+}(aq) + 2\ e^-$	$\rightarrow Hg(\ell)$	+0.855
$Ag^+(aq) + e^-$	$\rightarrow Ag(s)$	+0.80
$Hg_2^{2+}(aq) + 2\ e^-$	$\rightarrow 2\ Hg(\ell)$	+0.789
$Fe^{3+}(aq) + e^-$	$\rightarrow Fe^{2+}(aq)$	+0.771
$I_2(s) + 2\ e^-$	$\rightarrow 2\ I^-(aq)$	+0.535
$O_2(g) + 2\ H_2O(\ell) + 4\ e^-$	$\rightarrow 4\ OH^-(aq)$	+0.40
$Cu^{2+}(aq) + 2\ e^-$	$\rightarrow Cu(s)$	+0.337
$Sn^{4+}(aq) + 2\ e^-$	$\rightarrow Sn^{2+}(aq)$	+0.15
$2\ H_3O^+(aq) + 2\ e^-$	$\rightarrow H_2(g) + 2\ H_2O(\ell)$	0.00
$Sn^{2+}(aq) + 2\ e^-$	$\rightarrow Sn(s)$	−0.14
$Ni^{2+}(aq) + 2\ e^-$	$\rightarrow Ni(s)$	−0.25
$V^{3+}(aq) + e^-$	$\rightarrow V^{2+}(aq)$	−0.255
$PbSO_4(s) + 2\ e^-$	$\rightarrow Pb(s) + SO_4^{2-}(aq)$	−0.356
$Cd^{2+}(aq) + 2\ e^-$	$\rightarrow Cd(s)$	−0.40
$Fe^{2+}(aq) + 2\ e^-$	$\rightarrow Fe(s)$	−0.44
$Zn^{2+}(aq) + 2\ e^-$	$\rightarrow Zn(s)$	−0.763
$2\ H_2O(\ell) + 2\ e^-$	$\rightarrow H_2(g) + 2\ OH^-(aq)$	−0.8277
$Al^{3+}(aq) + 3\ e^-$	$\rightarrow Al(s)$	−1.66
$Mg^{2+}(aq) + 2\ e^-$	$\rightarrow Mg(s)$	−2.37
$Na^+(aq) + e^-$	$\rightarrow Na(s)$	−2.714
$K^+(aq) + e^-$	$\rightarrow K(s)$	−2.925
$Li^+(aq) + e^-$	$\rightarrow Li(s)$	−3.045

[61]